THE JOURNAL OF PHYSICAL CHEMISTRY Letters

Letter

Cite This: J. Phys. Chem. Lett. 2018, 9, 7160−7164

pubs.acs.org/JPCL

Origin of Two-Dimensional Vertical Ferroelectricity in WTe_2 Bilayer and Multilayer

Qing Yang,[†] Menghao Wu,*[,†] and Ju Li*[,‡]

[†]School of Physics, Huazhong University of Science and Technology, Wuhan, Hubei 430074, China

[‡]Department of Nuclear Science and Engineering and Department of Materials Science and Engineering, Massachusetts Institute of Technology, Cambridge, Massachusetts 02139, United States

Supporting Information

ABSTRACT: In a recent report, room-temperature vertical ferroelectricity was experimentally shown in WTe_2 bilayer, while its mechanism of ferroelectric switching without vertical ion displacements remains unclarified. In this work, we reveal its origin by first-principles calculations that the polarization stems from uncompensated interlayer vertical charge transfer depending on in-plane translation, which can be switched upon interlayer sliding. The calculated results are consistent with experimental data, and a similar switching mechanism can be applied to a multilayer counterpart. Despite its small ferroelectric switching barrier and polarization, the in-plane rigidity of WTe_2 layer gives rise to a high Curie temperature. A moire pattern of ferroelectric domain superlattice can be formed and tuned upon a small-angle twist of bilayer, which is unique compared with traditional ferroelectrics. Similar interlayer translational ferroelectricity may exist in a series of van der Waals bilayers or even bulk phases.

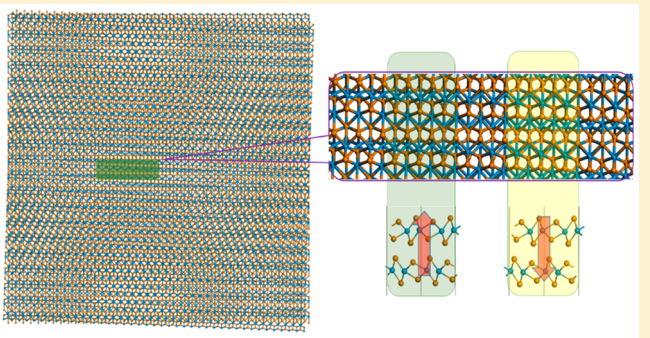

Two-dimensional (2D) materials like graphene,[1] transition-metal dichalcogenide,[2] and phosphorene,[3] with atomic thickness and high mobility, are promising candidates to replace the current semiconductor materials in microelectronics and to sustain Moore's law for a longer time. For their combination with nonvolatile memories, ferromagnetism (FM) and ferroelectricity (FE) in 2D materials have become two research foci in recent years. Although FM had been predicted in various 2D systems in the past decade,[4] it was not until in 2017 that 2D FM was experimentally verified in CrI_3[5] and $Cr_2Ge_2Te_6$,[6] with both measured Curie temperatures below ∼45 K. In comparison, the predictions of FE in 2D materials date back only to 2013[7−13] with the experimental realizations in 2016.[14,15] However, the Curie temperature of all those 2D FE systems were measured to be above room-temperature, including $CuInP_2S_6$,[16] In_2Se_3,[17,18] and IV−VI group compound,[14,19] as summarized in our recent review.[20] This can be attributed to the difference in switching barrier between 2D FM and 2D FE: the energy barrier of spin-flipping in 2D FM is usually below a tenth of a millielectronvolt especially in semiconductors, while the dipole switching barrier in 2D FE may reach hundreds of millielectronvolts. Compared with traditional FE like perovskites or PVDF with large bandgaps and poor electron mobility, the 2D FE may render a much better combination of nanocircuits based on high-mobility semiconductors and a much enhanced integration density. The van der Waals interaction at the interface between 2D FE and 3D semiconductors also allow lattice mismatch for epitaxial growth, while the epitaxial growth of perovskites on silicon is hindered by such issue of lattice mismatch.

A very recent study[21] further demonstrated the out-of-plane switchable polarization in two- or three-layer WTe_2, although WTe_2 is well-known as a topological semimetal in previous reports.[22−24] Despite the polarization that was almost negligible compared with traditional perovskite FE (3 orders of magnitude lower than $BaTiO_3$), the Curie temperature amazingly turned out to be around 350 K. The origin of such FE is still unclarified, as the vertical polarization seems to be switchable without vertical ion displacement. It was supposed in this report that the FE may origin from the electron−hole correlation rather than lattice instability, where a relative motion of the electron cloud relative to the ion core may take place.[21] Here we show first-principles evidence that the weak FE should stem from interlayer sliding, akin to previously predicted FE in van der Waals bilayer like BN or MoS_2,[25] where the vertical polarization and interlayer translation are coupled. The vertical polarization can be switched upon in-plane ion displacement, which will not be screened as it is metallic in-plane while the electrons are confined vertically. The in-plane rigidity of WTe_2 layer makes the antiferroelectric configuration highly unfavorable in energy and gives rise to a high Curie temperature.

Received: December 5, 2018
Accepted: December 12, 2018
Published: December 12, 2018

DOI: 10.1021/acs.jpclett.8b03654
J. Phys. Chem. Lett. 2018, 9, 7160−7164

The geometric structure of WTe_2 bilayer denoted as state I is displayed in Figure 1a, and an equivalent state II with

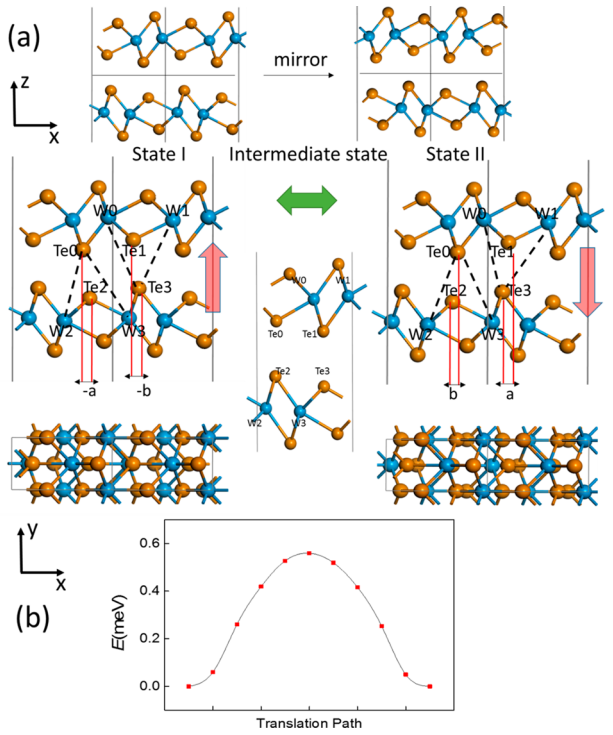

Figure 1. (a) Geometric structure of state I of WTe_2 bilayer and state II obtained by reflecting state I across the central horizontal plane, which can be also obtained by interlayer translation. (b) FE switching pathway of WTe_2 bilayer from state I to state II. Blue and orange spheres denote W and Te atoms respectively, and red arrows denote the polarization direction.

reversed vertical polarization can be obtained via mirror operation on state I with respect to the horizontal plane in the center. The horizontal polarization will not be reversed from I to II since the mirror operation is with respect to a horizontal plane. Meanwhile we note that only a slight interlayer translation is required to transform state I to state II, which may render a feasible FE switching pathway. As displayed for state I, along the $-x$ direction, the horizontal distance between Te0 and Te2, $x(\mathrm{Te0}) - x(\mathrm{Te2}) = -a = -0.32$ Å, is slightly distinct from the horizontal distance between Te1 and Te3, $x(\mathrm{Te1}) - x(\mathrm{Te3}) = -b = -0.40$ Å; state II can be obtained via moving the upper layer along the $-x$ axis by a distance of $a + b = 0.72$ Å, where the horizontal distance $x(\mathrm{Te0}) - x(\mathrm{Te2})$ and $x(\mathrm{Te1}) - x(\mathrm{Te3})$ in state II will respectively switch to $b = 0.40$ Å and $a = 0.32$ Å.

On the basis of our nudge-elastic-band (NEB) calculation of the FE switching minimum energy pathway in Figure 1b, the energy barrier for such slippage-induced polarization transition is only ~0.6 meV per unit cell. The intermediate state is nonpolar where the two layers are equivalent and the horizontal distance $x(\mathrm{Te0}) - x(\mathrm{Te2})$ and $x(\mathrm{Te1}) - x(\mathrm{Te3})$ are respectively $(b - a)/2$ and $(a - b)/2$. For example, the positions of Te0 and Te3 are completely equivalent and their charges are both 0.075e by Hirshfeld analysis. In comparison, the charges on Te0 and Te3 are respectively 0.077 and 0.073e in state I, as the upper and down layer become nonequivalent due to the broken symmetry: the interlayer Te−W distance, Te0−W2 and Te0−W3 are respectively 5.02 and 5.71 Å, while Te3−W0 and Te3−W1 are respectively 5.23 and 5.42 Å; for state II, the Te0−W2/W3 distance will swap with Te3−W0/W1, and the charges on Te0 will swap with Te3. The nonequivalence of two layers gives rise to an uncompensated charge transfer and a vertical polarization, which switches from upward at state I to downward at state II. Figure S1 displays the bandstructure of WTe_2 bilayer, where the slight Rashba splitting also indicates the breaking of symmetry and the possibility of tuning spin by electric field. Our results show that the vertical FE polarization of WTe_2 bilayer is around 3.2×10^{11} e/cm^2, which is consistent with the value of 2×10^{11} e/cm^2 measured at 20 K by experiment, considering the thermal fluctuation and possible defects.

To make sure state I is not the local minimum but the ground state, the energy dependences on interlayer translation along the $-x$ and $-y$ directions are plotted in parts a and b of Figure 2, where x and y are respectively denoted as the interlayer displacement along $-x$ and $-y$ direction compared with the intermediate state $(x = 0, y = 0)$. The energy profile of WTe_2 bilayer along -x direction reveals a double-well potential of ferroelectrics, where the energy minimum locates at $x = \pm(a + b)/2 = \pm 0.36$ Å, which is not the maximum point for polarization: the FE polarization can be further enhanced via interlayer translation along the $-x$ direction, which can reach its maximum value that is almost doubled at $x = \pm 0.90$ Å, as shown in Figure 2a. In comparison, the energy minimum locates at $y = 0$ along the $-y$ direction in Figure 2b, which is also the point where the polarization reaches its maximum. The oscillating polarization upon translation may be utilized as proposed previously,[25] as shown in Figure S2: when the upper layer is dragged along either the $-x$ or $-y$ direction, the interlayer voltage will oscillate and generate an alternating current output signal, which can be used as nanogenerator, where variations in the potential of the bilayer system can be used to drive the flow of electrons and harvest energies. It is also worth to note that the vertical polarization can be further enhanced if the interlayer distance is compressed due to enhanced interlayer charge-transfer, as shown in Figure 2c, which can increase by ~50% upon a 7% compression of interlayer distance.

The FE induced by interlayer sliding may be experimentally verified using scanning transmission electron microscope (STEM) as the change of bilayer nanostructure after FE switching can be characterized. Similar FE switching mechanism can be applied to multilayer which maintains 1T' structure. As shown in Figure 3, the polarization of WTe_2 trilayer can be switched from downward to upward as the middle layer displaced by $a + b$, and the switchable polarization of WTe_2 trilayer is around 2.2×10^{11} e/cm^2. For the case of five layer, its polarization will be switched as the second and fourth layer displaced by $a + b$ simultaneously. Akin to previously predicted low-dimensional metallic multiferroics,[25−28] the thin-layer WTe_2 are metallic in-plane while the electrons are confined vertically, so the vertical polarization can be switchable in thin-layer while external electric field may be screened in its metallic bulk phase. However, for insulating van der Waals 1T' layers with a similar $Pnm2_1$ structure like ZrI_2, their bulk phase may also be FE with switchable polarizations.

To investigate the stability of FE state, we also take possible antiferroelectric (AFE) configurations into account. Here the vertical polarization stems from interlayer translation, which is uniform as each layer is almost rigid in plane, making AFE

DOI: 10.1021/acs.jpclett.8b03654
J. Phys. Chem. Lett. 2018, 9, 7160−7164

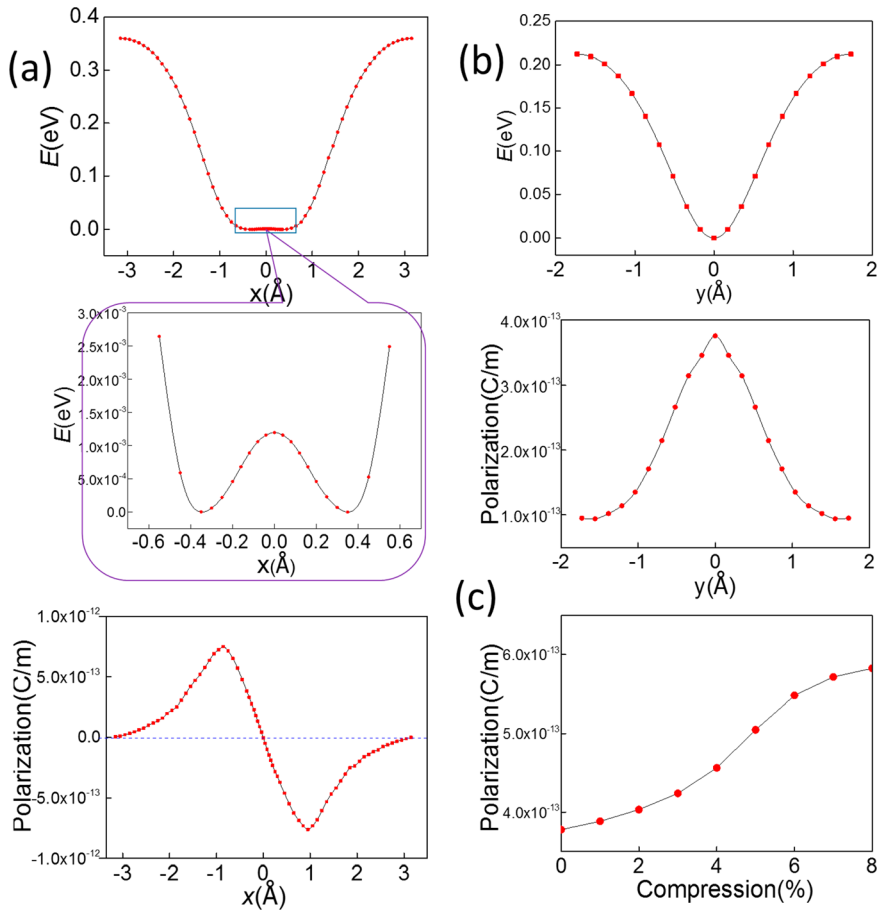

Figure 2. (a) Dependence of energy and polarization on x along the $-x$ direction at $y = 0$. (b) Dependence of energy and polarization on y along the $-y$ direction at $x = -(a + b)/2$. (c) Dependence of polarization on the compression of interlayer distance of the WTe_2 bilayer.

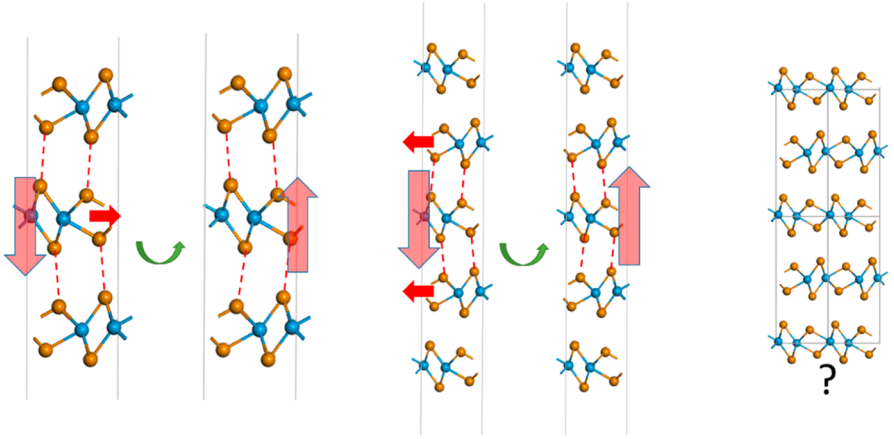

Figure 3. FE switching of WTe_2 trilayer, five-layer, and bulk phase structure.

configuration highly unstable. In Figure 4a, we obtain an unstable artificial AFE phase by doubling the unit cell along the $-x$ direction, where the translation is positive in one unit cell but negative in the other with opposite vertical polarizations. This AFE state is 0.39 eV/f.u. higher in energy compared with the FE ground state, which can clarify why Curie temperature still over 350 K despite the polarization (3.2×10^{11} e/cm^2 = 5.1×10^{-2} μC/cm^2) and FE switching barrier (~0.6 meV) that both are almost negligible. Here the FE switching barrier is the "collective" barrier where all dipoles must "simultaneously" switch to the opposite direction; however, the Curie temperature mainly depends on the "isolated" barrier Δ for one dipole to flip while all other dipoles around are fixed ($T_c \approx \frac{2\Delta}{3k_B}$ for a coarse estimation[29,30]), and the in-plane rigidity of WTe_2 layer will give rise to a large "isolated" barrier Δ.

Although the AFE state is highly unstable, the FE domains of opposite directions can be formed upon a small angle twist within the bilayer, as shown in Figure 4b, giving rise to a Moire superlattice pattern with superlattice period $L \propto l/\theta$. If a twisted angle as small as $\theta = 0.2°$ can be obtained in such bilayer as reported in a recent experiment,[31] this domain size

DOI: 10.1021/acs.jpclett.8b03654
J. Phys. Chem. Lett. 2018, 9, 7160−7164

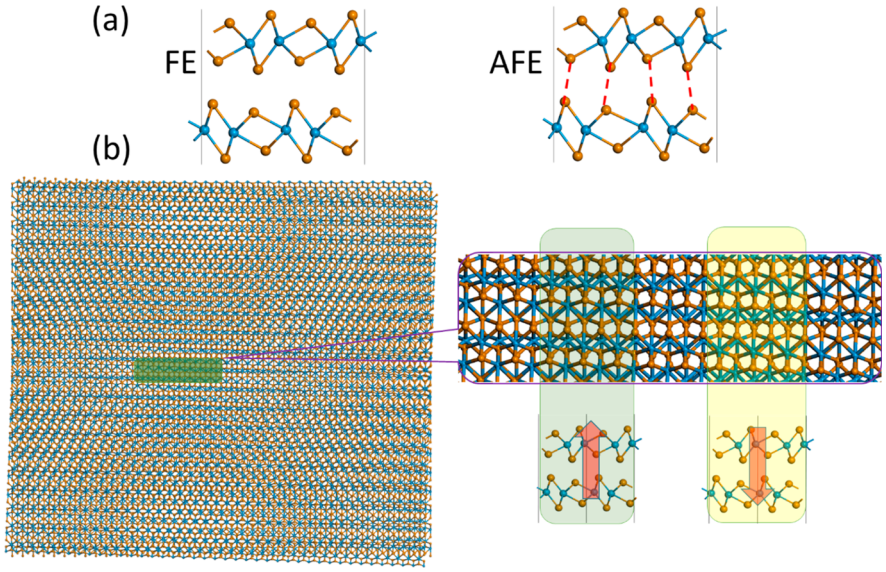

Figure 4. (a) Geometric structure of FE and artificial AFE configuration. (b) FE domains formed by moire patterns upon a small angle twist of bilayer.

will be over 180 nm. Similar to previous design of exciton funnel by a spatially varying bandgap in a twisted bilayer,[32] an internal stacking translation $\mathbf{u}(\mathbf{r})$ varying gently with position $\mathbf{r}$ can be created and control the local polarization $P(\mathbf{u}(\mathbf{r}))$. P will be upward when $\mathbf{u}_x(\mathbf{r}) > 0$, and downward when $\mathbf{u}_x(\mathbf{r}) < 0$. The adsorption of certain dipole molecules that assemble only in certain domains may even give rise to molecular superlattice with novel properties.

In summary, we show first-principles evidence that the polarization of WTe_2 bilayer stems from uncompensated interlayer vertical charge transfer depending on in-plane slippage, which can be verified by using in situ transmission electron microscopy,[33] and the computed results are consistent with the experiment. It is metallic in-plane while the electrons are confined vertically, so the vertical polarization can be switchable upon interlayer sliding for thin-layer, while external electric field may be screened in its bulk phase. The in-plane rigidity of WTe_2 layer makes the AFE configuration highly unstable, which clarifies the origin of high Curie temperature despite the negligible FE switching barrier and polarization. A Moire superlattice pattern of FE domains can be formed and tuned upon a small angle twist of bilayer, which is unique compared with traditional ferroelectrics. Once there is slippage, the two layers are no longer equivalent; because the dependence of charge transfer on in-plane slippage is generic, similar ferroelectric effect induced by interlayer translation and rotation is predicted to exist widely in various other van der Waals (BN, MoS_2, GaSe, MXene, etc.[25]) bilayers or even bulk phases.

Our density function theory (DFT) calculations are carried out using the Vienna ab initio simulation package (VASP).[34,35] The projector augmented wave (PAW) potentials[36] and the generalized gradient approximation (GGA) in the Perdew–Burke–Ernzerhof (PBE) form[37] are applied. The plane-wave cutoff energy for wave function is set to 500 eV. For the geometry optimization, PBE-D3 method of Grimme with BJ damping[38] is applied for taking van der Waals interaction into account. 11× 7 × 1 Monkhorst–Pack k-meshes are adopted for bilayer structures and a vacuum spacing of ∼17 Å is used. For ground states like I and II, both lattice constants and atomic positions are relaxed until the residual force on atoms are less than 0.001 eV/ Å during optimization. Dipole moment correction is employed to evaluate the vertical polarization, and the FE switching pathway is obtained by using the nudged elastic band (NEB) method.[39]

■ ASSOCIATED CONTENT

Supporting Information

The Supporting Information is available free of charge on the ACS Publications website at DOI: 10.1021/acs.jpclett.8b03654.

Band structure and model of nanogenerator based on WTe_2 bilayer; atomic coordinates of WTe_2 multilayer (PDF)

■ AUTHOR INFORMATION

Corresponding Authors

*E-mail: wmh1987@hust.edu.cn (M.W.).
*E-mail: liju@mit.edu (J.L.).

ORCID

Menghao Wu: 0000-0002-1683-6449
Ju Li: 0000-0002-7841-8058

Notes

The authors declare no competing financial interest.

■ ACKNOWLEDGMENTS

We are supported by the National Natural Science Foundation of China (Nos. 21573084). We thank Prof. Junming Liu for helpful discussions and the Shanghai Supercomputing Center for providing computational resources. J.L. acknowledges support by NSF ECCS-1610806.

■ REFERENCES

(1) Novoselov, K. S.; Geim, A. K.; Morozov, S. V.; Jiang, D.; Zhang, Y.; Dubonos, S. V.; Grigorieva, I. V.; Firsov, A. A. Electric Field Effect in Atomically Thin Carbon Films. *Science* **2004**, *306* (5696), 666–669.

DOI: 10.1021/acs.jpclett.8b03654
J. Phys. Chem. Lett. 2018, 9, 7160–7164

(2) Radisavljevic, B.; Radenovic, A.; Brivio, J.; Giacometti, V.; Kis, A. Single-layer MoS2 transistors. *Nat. Nanotechnol.* **2011**, *6* (3), 147−150.
(3) Li, L.; Yu, Y.; Ye, G. J.; Ge, Q.; Ou, X.; Wu, H.; Feng, D.; Chen, X. H.; Zhang, Y. Black phosphorus field-effect transistors. *Nat. Nanotechnol.* **2014**, *9* (5), 372−377.
(4) Li, X.; Wu, X. Two-dimensional monolayer designs for spintronics applications. *Wiley Interdisciplinary Reviews: Computational Molecular Science* **2016**, *6* (4), 441−455.
(5) Huang, B.; Clark, G.; Navarro-Moratalla, E.; Klein, D. R.; Cheng, R.; Seyler, K. L.; Zhong, D.; Schmidgall, E.; McGuire, M. A.; Cobden, D. H.; Yao, W.; Xiao, D.; Jarillo-Herrero, P.; Xu, X. Layer-dependent ferromagnetism in a van der Waals crystal down to the monolayer limit. *Nature* **2017**, *546* (7657), 270−273.
(6) Gong, C.; Li, L.; Li, Z.; Ji, H.; Stern, A.; Xia, Y.; Cao, T.; Bao, W.; Wang, C.; Wang, Y.; Qiu, Z. Q.; Cava, R. J.; Louie, S. G.; Xia, J.; Zhang, X. Discovery of intrinsic ferromagnetism in two-dimensional van der Waals crystals. *Nature* **2017**, *546* (7657), 265−269.
(7) Wu, M.; Burton, J. D.; Tsymbal, E. Y.; Zeng, X. C.; Jena, P. Hydroxyl-decorated graphene systems as candidates for organic metal-free ferroelectrics, multiferroics, and high-performance proton battery cathode materials. *Phys. Rev. B: Condens. Matter Mater. Phys.* **2013**, *87* (8), 081406.
(8) Wu, M.; Dong, S.; Yao, K.; Liu, J.; Zeng, X. C. Ferroelectricity in Covalently functionalized Two-dimensional Materials: Integration of High-mobility Semiconductors and Nonvolatile Memory. *Nano Lett.* **2016**, *16* (11), 7309−7315.
(9) Shirodkar, S. N.; Waghmare, U. V. Emergence of Ferroelectricity at a Metal-Semiconductor Transition in a 1T Monolayer of MoS_2. *Phys. Rev. Lett.* **2014**, *112* (15), 157601.
(10) Di Sante, D.; Stroppa, A.; Barone, P.; Whangbo, M.-H.; Picozzi, S. Emergence of ferroelectricity and spin-valley properties in two-dimensional honeycomb binary compounds. *Phys. Rev. B: Condens. Matter Mater. Phys.* **2015**, *91* (16), 161401.
(11) Zhao, Y.; Lin, L.; Zhou, Q.; Li, Y.; Yuan, S.; Chen, Q.; Dong, S.; Wang, J. Surface Vacancy-Induced Switchable Electric Polarization and Enhanced Ferromagnetism in Monolayer Metal Trihalides. *Nano Lett.* **2018**, *18* (5), 2943−2949.
(12) Huang, C.; Du, Y.; Wu, H.; Xiang, H.; Deng, K.; Kan, E. Prediction of Intrinsic Ferromagnetic Ferroelectricity in a Transition-Metal Halide Monolayer. *Phys. Rev. Lett.* **2018**, *120* (14), 147601.
(13) Tu, Z.; Wu, M.; Zeng, X. C. Two-Dimensional Metal-Free Organic Multiferroic Material for Design of Multifunctional Integrated Circuits. *J. Phys. Chem. Lett.* **2017**, *8* (9), 1973−1978.
(14) Chang, K.; Liu, J.; Lin, H.; Wang, N.; Zhao, K.; Zhang, A.; Jin, F.; Zhong, Y.; Hu, X.; Duan, W.; Zhang, Q.; Fu, L.; Xue, Q.-K.; Chen, X.; Ji, S.-H. Discovery of robust in-plane ferroelectricity in atomic-thick SnTe. *Science* **2016**, *353* (6296), 274.
(15) Liu, F.; You, L.; Seyler, K. L.; Li, X.; Yu, P.; Lin, J.; Wang, X.; Zhou, J.; Wang, H.; He, H.; Pantelides, S. T.; Zhou, W.; Sharma, P.; Xu, X.; Ajayan, P. M.; Wang, J.; Liu, Z. Room-temperature ferroelectricity in CuInP2S6 ultrathin flakes. *Nat. Commun.* **2016**, *7*, 12357.
(16) Belianinov, A.; He, Q.; Dziaugys, A.; Maksymovych, P.; Eliseev, E.; Borisevich, A.; Morozovska, A.; Banys, J.; Vysochanskii, Y.; Kalinin, S. V. CuInP2S6 Room Temperature Layered Ferroelectric. *Nano Lett.* **2015**, *15* (6), 3808−3814.
(17) Zhou, Y.; Wu, D.; Zhu, Y.; Cho, Y.; He, Q.; Yang, X.; Herrera, K.; Chu, Z.; Han, Y.; Downer, M. C.; Peng, H.; Lai, K. Out-of-Plane Piezoelectricity and Ferroelectricity in Layered alpha-In2Se3 Nanoflakes. *Nano Lett.* **2017**, *17* (9), 5508−5513.
(18) Ding, W.; Zhu, J.; Wang, Z.; Gao, Y.; Xiao, D.; Gu, Y.; Zhang, Z.; Zhu, W. Prediction of intrinsic two-dimensional ferroelectrics in In2Se3 and other III2-VI3 van der Waals materials. *Nat. Commun.* **2017**, *8*, 14956.
(19) Wu, M.; Zeng, X. C. Intrinsic Ferroelasticity and/or Multiferroicity in Two-Dimensional Phosphorene and Phosphorene Analogues. *Nano Lett.* **2016**, *16* (5), 3236−3241.
(20) Wu, M.; Jena, P. The rise of two-dimensional van der Waals ferroelectrics. *Wiley Interdisciplinary Reviews: Computational Molecular Science* **2018**, *8* (5), No. e1365.
(21) Fei, Z.; Zhao, W.; Palomaki, T. A.; Sun, B.; Miller, M. K.; Zhao, Z.; Yan, J.; Xu, X.; Cobden, D. H. Ferroelectric switching of a two-dimensional metal. *Nature* **2018**, *560* (7718), 336−339.
(22) Qian, X.; Liu, J.; Fu, L.; Li, J. Quantum spin Hall effect in two-dimensional transition metal dichalcogenides. *Science* **2014**, *346* (6215), 1344−1347.
(23) Yang, J.; Jin, Y.; Xu, W.; Zheng, B.; Wang, R.; Xu, H. Oxidation-Induced Topological Phase Transition in Monolayer 1T′-WTe2. *J. Phys. Chem. Lett.* **2018**, *9* (16), 4783−4788.
(24) Kou, L.; Ma, Y.; Sun, Z.; Heine, T.; Chen, C. Two-Dimensional Topological Insulators: Progress and Prospects. *J. Phys. Chem. Lett.* **2017**, *8* (8), 1905−1919.
(25) Li, L.; Wu, M. Binary Compound Bilayer and Multilayer with Vertical Polarizations: Two-Dimensional Ferroelectrics, Multiferroics, and Nanogenerators. *ACS Nano* **2017**, *11* (6), 6382−6388.
(26) Wu, M.; Burton, J. D.; Tsymbal, E. Y.; Zeng, X. C.; Jena, P. Multiferroic Materials Based on Organic Transition-Metal Molecular Nanowires. *J. Am. Chem. Soc.* **2012**, *134* (35), 14423−14429.
(27) Yang, Q.; Xiong, W.; Zhu, L.; Gao, G.; Wu, M. Chemically Functionalized Phosphorene: Two-Dimensional Multiferroics with Vertical Polarization and Mobile Magnetism. *J. Am. Chem. Soc.* **2017**, *139* (33), 11506−11512.
(28) Luo, W.; Xu, K.; Xiang, H. Two-dimensional hyperferroelectric metals: A different route to ferromagnetic-ferroelectric multiferroics. *Phys. Rev. B: Condens. Matter Mater. Phys.* **2017**, *96* (23), 235415.
(29) Wu, M.; Duan, T.; Lu, C.; Fu, H.; Dong, S.; Liu, J. Proton transfer ferroelectricity/multiferroicity in rutile oxyhydroxides. *Nanoscale* **2018**, *10* (20), 9509−9515.
(30) Wu, M.; Zeng, X. C.; Jena, P. Unusual Magnetic Properties of Functionalized Graphene Nanoribbons. *J. Phys. Chem. Lett.* **2013**, *4* (15), 2482−2488.
(31) Ribeiro-Palau, R.; Zhang, C.; Watanabe, K.; Taniguchi, T.; Hone, J.; Dean, C. R. Twistable electronics with dynamically rotatable heterostructures. *Science* **2018**, *361* (6403), 690−693.
(32) Wu, M.; Qian, X.; Li, J. Tunable Exciton Funnel Using Moiré Superlattice in Twisted van der Waals Bilayer. *Nano Lett.* **2014**, *14* (9), 5350−5357.
(33) Kushima, A.; Qian, X.; Zhao, P.; Zhang, S.; Li, J. Ripplocations in van der Waals Layers. *Nano Lett.* **2015**, *15* (2), 1302−1308.
(34) Kresse, G.; Furthmüller, J. Efficiency of ab-initio total energy calculations for metals and semiconductors using a plane-wave basis set. *Comput. Mater. Sci.* **1996**, *6* (1), 15−50.
(35) Kresse, G.; Furthmüller, J. Efficient iterative schemes for ab initio total-energy calculations using a plane-wave basis set. *Phys. Rev. B: Condens. Matter Mater. Phys.* **1996**, *54* (16), 11169−11186.
(36) Blöchl, P. E. Projector augmented-wave method. *Phys. Rev. B: Condens. Matter Mater. Phys.* **1994**, *50* (24), 17953−17979.
(37) Perdew, J. P.; Burke, K.; Ernzerhof, M. Generalized Gradient Approximation Made Simple. *Phys. Rev. Lett.* **1996**, *77* (18), 3865−3868.
(38) Grimme, S.; Ehrlich, S.; Goerigk, L. Effect of the damping function in dispersion corrected density functional theory. *J. Comput. Chem.* **2011**, *32* (7), 1456−1465.
(39) Henkelman, G.; Uberuaga, B. P.; Jónsson, H. A climbing image nudged elastic band method for finding saddle points and minimum energy paths. *J. Chem. Phys.* **2000**, *113* (22), 9901−9904.

DOI: 10.1021/acs.jpclett.8b03654
J. Phys. Chem. Lett. 2018, 9, 7160−7164

Supporting Information

The Origin of Two-dimensional Vertical Ferroelectricity in WTe_2 Bilayer and Multilayer

Qing Yang[1], Menghao Wu[1]* and Ju Li[2]*

[1]School of Physics, Huazhong University of Science and Technology, Wuhan, Hubei 430074, China

[2]Department of Nuclear Science and Engineering and Department of Materials Science and Engineering, Massachusetts Institute of Technology, Cambridge, MA 02139, USA

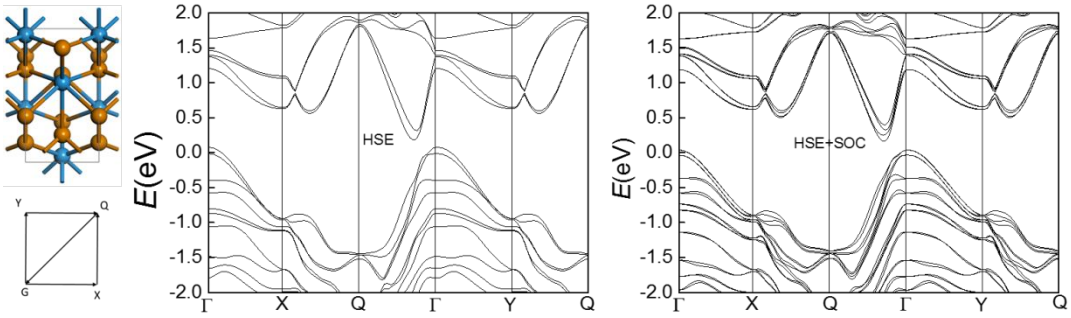

Figure S1. Bandstructure of WTe_2 bilayer using HSE hybrid functional without (left) and with (right) spin-orbit-coupling (SOC).

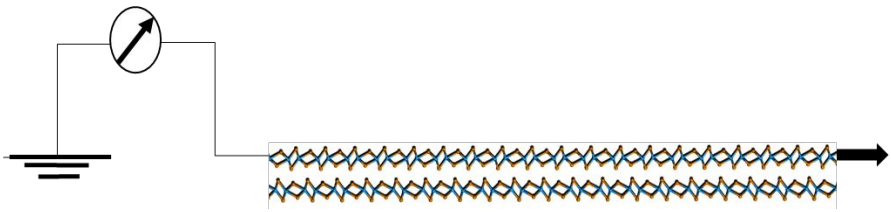

Figure S2. A model of nanogenerator based on WTe_2 bilayer.

Atomic coordinates of WTe_2 bilayer

1.00000000000000

3.4607000350999999 0.0000000000000000 0.0000000000000000

0.0000000000000000 6.2870001792999997 0.0000000000000000

0.0000000000000000 0.0000000000000000 27.6956005095999984

Te W

8 4

Direct

0.0000000000000000 0.9012284753509948 0.3946230883458361

0.0000000000000000 0.6961558320747826 0.6206226121463042

0.5000000000000000 0.2001987452294568 0.6439784410384347

0.5000000000000000 0.4088910096420370 0.3725928912811385

0.5000000000000000 0.8506600095301939 0.7722213485511918

0.5000000000000000 0.7588142335939373 0.5008885885421430

0.0000000000000000 0.2508067906982924 0.5241123163409787

0.0000000000000000 0.3442652811477714 0.7501597104027923

0.0000000000000000 0.9509472064109632 0.7003452704765928

0.0000000000000000 0.5086180436370058 0.4445564448031266

0.5000000000000000 0.1513524174977098 0.4520170329204892

0.5000000000000000 0.5936319321868546 0.6926122341509657

Atomic coordinates of WTe_2 trilayer

1.00000000000000

3.4782434116565160 0.0000000000000000 0.0000000000000000

0.0000000000000000 6.2686937481304170 0.0000000000000000

0.0000000000000000 0.0000000000000000 39.7021913604521046

Te W

12 6

Direct

0.0000000000000000 0.7862825825780726 0.2731442378205124

0.0000000000000000 0.6934417686506350 0.4293051916446707

0.5000000000000000 0.1995267348113455 0.4456567642543064

0.5000000000000000 0.2921321898865364 0.2577830776533079

0.5000000000000000 0.8488691057635033 0.5351275283140976

0.5000000000000000 0.6404421813934271 0.3469701094844209

0.0000000000000000 0.1369030929418237 0.3634175005153105

0.0000000000000000 0.3457448527112491 0.5186577001606389

0.0000000000000000 0.7860900312584480 0.6170233921535691

0.5000000000000000 0.2944370011834427 0.6006750867414904

0.5000000000000000 0.6419209487867330 0.6908986089121893

0.0000000000000000 0.1345313927591505 0.7062102453272686

0.0000000000000000 0.9504576085332562 0.4849981579704231

0.0000000000000000 0.3919100487200315 0.3078258833231889

0.5000000000000000 0.0347828734747544 0.3133373434836297

0.5000000000000000 0.5946028068815488 0.4794418261232885

0.0000000000000000 0.3925868033131955 0.6508409277455465

0.5000000000000000 0.0356279053528466 0.6560763973721453

Atomic coordinates of WTe2 four-layer

1.00000000000000

3.4899439911561587 0.0000000000000000 0.0000000000000000

0.0000000000000000 6.2701544592006861 0.0000000000000000

0.0000000000000000 0.0000000000000000 54.3633927331867213

Te W

16 8

Direct

0.0000000000000000 0.7873201020769610 0.1967933845281793

0.0000000000000000 0.6946937680620540 0.3103696924734822

0.5000000000000000 0.2003900385293076 0.3223619283724699

0.5000000000000000 0.2924121939470777 0.1855360393046575

0.5000000000000000 0.8500447410722639 0.3875434548070380

0.5000000000000000 0.6403153779247702 0.2505265110442350

0.0000000000000000 0.1375009087133538 0.2625915197241135

0.0000000000000000 0.3471656069774543 0.3754075530341398

0.0000000000000000 0.7851141061773658 0.4470078369712135

0.0000000000000000 0.6920684634872065 0.5599865149035973

0.5000000000000000 0.2002079657957500 0.5719241134623674

0.5000000000000000 0.2918552343016661 0.4349578519053344

0.5000000000000000 0.8524860067108975 0.6369578900533119

0.5000000000000000 0.6386776895077607 0.5000797286218331

0.0000000000000000 0.1356880849084104 0.5121111068888284

0.0000000000000000 0.3453539894525958 0.6257517281018603

0.0000000000000000 0.9515808828896133 0.3510107395081743

0.0000000000000000 0.3921811402408639 0.2220217356443556

0.5000000000000000 0.0353126799037148 0.2260944732145339

0.5000000000000000 0.5958952959262567 0.3469195634743548

0.0000000000000000 0.9511502990775857 0.6003967467286651

0.0000000000000000 0.3899531686337772 0.4715167724502209

0.5000000000000000 0.0341955348354600 0.4755312294152497

0.5000000000000000 0.5943166508478299 0.5965618203677960